

UDC 621.316.728

https://doi.org/10.33619/2414-2948/103/40

ENERGY CIRCUIT OF A THERMAL CIRCUIT WITH A DIRECT-ACTING REGULATOR WITH A CAPACITY OF 1 MW IN PULSATING MODE

©*Han Wang*, ORCID: 0009-0004-8789-0217, Ogarev Mordovia State University,
Saransk, Russia, wh2244566@gmail.com

©*Maltsev S.*, ORCID: 0009-0005-7485-0352, SPIN-code: 9830-6014, Ph.D.,
Ogarev Mordovia State University, Saransk, Saransk, Russia, malcevca@mail.ru

ЭНЕРГЕТИЧЕСКАЯ СХЕМА ТЕПЛОВОЙ ЦЕПИ С РЕГУЛЯТОРОМ ПРЯМОГО ДЕЙСТВИЯ МОЩНОСТЬЮ 1 МВт В ПУЛЬСИРУЮЩЕМ РЕЖИМЕ

©*Хань Ван*, ORCID: 0009-0004-8789-0217, Национальный исследовательский Мордовский
государственный университет им. Н.П. Огарева, Саранск, Россия, wh2244566@gmail.com

©*Мальцев С. А.*, ORCID: 0009-0005-7485-0352, SPIN-код: 9830-6014, канд. техн. наук,
Национальный исследовательский Мордовский государственный университет
им. Н.П. Огарева, Саранск, Россия, malcevca@mail.ru

Abstract. The purpose of the work is to describe the installation using differential equations and obtain approximate values before the experiment. In this paper, a constructive scheme of the experimental device is proposed, and the principle of its operation is described in detail. The power circuit of the device has been drawn up. Complex impedance, frequency function, amplitude-frequency characteristic and phase-frequency characteristic are obtained by mathematical transformation of the power circuit. The frequency response of the circuit is constructed. As a result of the calculations, we will obtain the amplitude frequency response and the phase frequency response. Using the found values of the characteristics, we will build graphs and draw conclusions about how the characteristics depend on the change in parameters and why the graph lines of the graphs are exactly the way they are.

Аннотация. Цель работы — описать установку с помощью дифференциальных уравнений и получить примерные значения перед экспериментом. В данной работе предложена конструктивная схема экспериментальной установки и подробно описан принцип ее работы. Составлена силовая схема устройства. Комплексное сопротивление, функция частоты, амплитудно-частотная характеристика и фазочастотная характеристика получаются путем математического преобразования силовой цепи. Построена частотная характеристика схемы. В результате вычислений получим АЧХ и ФЧХ. Используя найденные значения характеристик, построим графики и сделаем выводы о том, как характеристики зависят от изменения параметров и почему линии графиков именно такие, какие они есть.

Keywords: hydraulic, heat exchanger, heat flow, heat transfer.

Ключевые слова: гидравлика, теплообменник, тепловой поток, теплопередача.

The energy circuit of a thermal system represents a crucial aspect of its operation, dictating the flow and distribution of energy within the system. In the context of thermal circuits employing direct-acting regulators, ensuring optimal energy management becomes paramount, particularly in scenarios characterized by pulsating modes of operation. This introduction delves into the intricacies of energy circulation within a thermal circuit featuring a direct-acting regulator with a

capacity of 1 MW operating in pulsating mode. By elucidating the interplay between energy input, regulation, and output, this discussion aims to shed light on the challenges and opportunities inherent in such systems. Through a comprehensive examination of the energy circuit dynamics and the role of the direct-acting regulator, this study endeavors to propose innovative solutions for enhancing system performance, efficiency, and reliability. The environment is very important [1].

In 2018, Xu [2] used a steam generator simulator to study the unsteady pressure pulsation characteristics of the reactor coolant pump at different flow rates and different rotational speeds. They used fast Fourier [3-11] transform and root mean square methods to analyze the pressure pulsation signals measured by sensors on the pump casing and oil outlet pipe. Under different flow rates, the pressure amplitude of FRPF increases with the increase of rotation speed, but the pressure amplitudes of FR and FSPF fluctuate slightly with the increase of rotation speed. Zhang [12] employed CFD numerical simulation to investigate the mechanics of non-uniform flow within the channel-head of the SG and discovered that the channel-head's asymmetric structure and the abrupt contraction of the connection between the channel-head and the inlet pipeline caused flow separation, resulting in non-uniform inflow. In 2024, Zhang [13] took the third-generation reactor RCP as the research object and used CFD to study the unsteady characteristics of the third-generation RCP under non-uniform inflow conditions, focusing on the pressure pulsation characteristics inside the RCP. It was found that non-uniform inflow can cause unstable pressure fluctuations in the "throat" area of the channel head.

The principle of operation of the experimental setup. Figure 1 shows an experimental setup for the ITP coolant supply regulator.

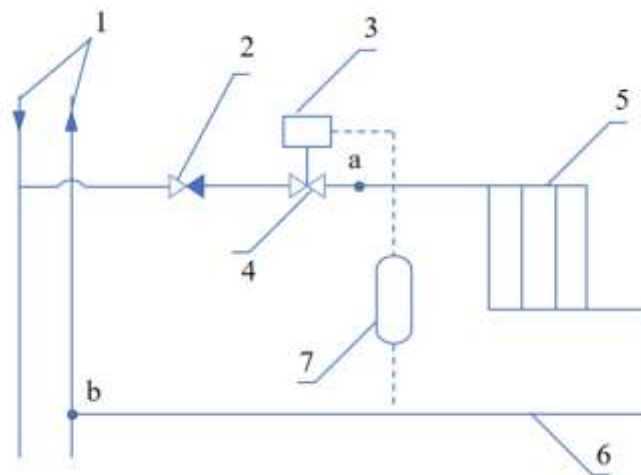


Figure 1. Experimental setup for the ITP coolant supply regulator: 1 – heating network; 2 – check valve; 3 – regulator; 4 – valve; 5 – heating devices; 6 – pipeline; 7 – sensor

Thermal energy comes from the heat network 1. The amount of thermal energy is regulated by the regulator 3, by a signal from the sensor 7. When the valve of the regulator 3 is closed, the flow rate and pressure on the heating device 5 will drop. Since the ambient air temperature is constantly changing, the regulator 3 always works.

In the course of the study, for a better understanding of the scheme, it was decided to study 2 characteristics of hydraulic and thermal, in order to better understand the nature of the forces arising and to more accurately determine the required parameters on the obtained model.

In the first power circuit the hydraulic characteristics at the moment of closing of the shock valve is considered. This circuit contains 3 elements.

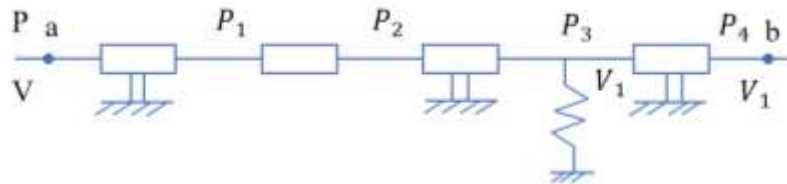


Figure 2. Hydraulic circuit

The circuit link equations:

$$\begin{cases} P = r_1 V^2 + m\dot{V} + r_2 V^2 + r_3 V_1^2 + P_4 \\ V = l\dot{P}_3 + V_1 \end{cases} \quad (1)$$

Equations for P_4, P_3, P_2, P_1 :

$$P_4 = P_{40} + \bar{P}_4 \quad (2)$$

$$P_3 = r_3 V_1^2 + P_4 \quad (3)$$

$$P_2 = r_2 V^2 + P_3 \quad (4)$$

$$P_1 = m\dot{V} + P_2 \quad (5)$$

Equations for V_1 :

$$V_1 = V_{10} + \bar{V}_1 \quad (6)$$

$$V_1^2 = V_{10}^2 + 2V_{10}\bar{V}_1 \quad (7)$$

Equation for P_3, \dot{P}_3 :

$$P_3 = r_3 V_1^2 + P_4 = r_3 V_{10}^2 + 2r_3 V_{10}\bar{V}_1 + P_{40} + \bar{P}_4 \quad (8)$$

$$\dot{P}_3 = 2r_3 V_{10}\dot{\bar{V}}_1 + \dot{\bar{P}}_4 \quad (9)$$

Equation for P_2 :

$$P_2 = r_2 V^2 + r_3 V_{10}^2 + 2r_3 V_{10}\bar{V}_1 + P_{40} + \bar{P}_4 \quad (10)$$

Equation for P_1 :

$$P_1 = m\dot{V} + r_2 V^2 + r_3 V_{10}^2 + 2r_3 V_{10}\bar{V}_1 + P_{40} + \bar{P}_4 \quad (11)$$

Equation for P :

$$P = (r_1 + r_2)V^2 + m\dot{V} + r_3 V_{10}^2 + 2r_3 V_{10}\bar{V}_1 + P_{40} + \bar{P}_4 \quad (12)$$

Equation for V :

$$V = l\dot{P}_3 + V_1 = 2lr_3 V_{10}\dot{\bar{V}}_1 + l\dot{\bar{P}}_4 + V_{10} + \bar{V}_1 \quad (13)$$

Equation for \dot{V} :

$$\dot{V} = 2lr_3 V_{10}\ddot{\bar{V}}_1 + l\ddot{\bar{P}}_4 + \dot{\bar{V}}_1 \quad (14)$$

Equation for V^2 :

$$V^2 = (V_{10} + 2lr_3 V_{10}\dot{\bar{V}}_1 + l\dot{\bar{P}}_4 + \bar{V}_1)^2 = V_{10}^2 + 4V_{10}^2 lr_3 \dot{\bar{V}}_1 + 4V_{10} l\dot{\bar{P}}_4 + 4V_{10}\bar{V}_1 \quad (15)$$

Equation for P :

$$P = (r_1 + r_2)(V_{10}^2 + 4V_{10}^2lr_3\ddot{V}_1 + 4V_{10}l\ddot{P}_4 + 4V_{10}\bar{V}_1) + m(2lr_3V_{10}\ddot{V}_1 + l\ddot{P}_4 + \dot{V}_1) + r_3V_{10}^2 + 2r_3V_{10}\bar{V}_1 \quad (16)$$

Equation for images:

$$(a_1s + a_2)V_1(s) = -(b_1s^2 + b_2s)P_4(s) \quad (17)$$

Coefficients:

$$\begin{aligned} a_1 &= 2lr_3V_{10} \\ a_2 &= 1 \\ b_1 &= ml \\ b_2 &= 4lr_2V_{10} \end{aligned} \quad (18)$$

Complex circuit resistance $Z(s)$:

$$Z(s) = \frac{P_4(s)}{V_1(s)} = \frac{a_1s + a_2}{-(b_1s^2 + b_2s)} \quad (19)$$

Frequency function of the circuit:

$$s \rightarrow j\Omega, j^2 = -1 \quad (20)$$

Frequency function of the circuit:

$$\begin{aligned} z(j\Omega) &= \frac{a_1j\Omega + a_2}{b_1\Omega^2 - b_2j\Omega} = \frac{(a_1j\Omega + a_2)(b_1\Omega^2 + b_2j\Omega)}{(b_1\Omega^2 - b_2j\Omega)(b_1\Omega^2 + b_2j\Omega)} \\ &= \frac{(a_1b_1j\Omega^3 - a_1b_2\Omega^2 + a_2b_1\Omega^2 + a_2b_2j\Omega)}{b_1^2\Omega^4 + b_2^2\Omega^2} \end{aligned} \quad (21)$$

The real part of the frequency function:

$$Re(j\Omega) = \frac{-a_1b_2\Omega^2 + a_2b_1\Omega^2}{b_1^2\Omega^4 + b_2^2\Omega^2} \quad (22)$$

Imaginary part of the frequency function:

$$Im(j\Omega) = \frac{a_1b_1\Omega^3 + a_2b_2\Omega}{b_1^2\Omega^4 + b_2^2\Omega^2} j \quad (23)$$

Amplitude-frequency response (frequency response) of the circuit:

$$A(j\Omega) = \sqrt{Re(j\Omega)^2 + Im(j\Omega)^2} \quad (24)$$

Phase frequency response (FFC) of the circuit:

$$\varphi(j\Omega) = -\arctg \frac{Im(j\Omega)}{Re(j\Omega)} \quad (25)$$

Calculate heat transfer energy circuit.

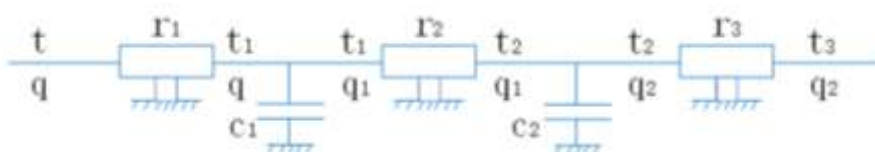


Figure 3. Heat transfer energy circuit

The circuit link equations:

$$\begin{cases} t = r_1 q + r_2 q_1 + r_3 q_2 + t_3 \\ q = c_1 \dot{t}_1 + c_2 \dot{t}_2 + q_2 \end{cases} \quad (26)$$

Equations for $t_3, t_2, \dot{t}_2, t_1, q_2$:

$$t_3 = t_{30} + \bar{t}_3 \quad (27)$$

$$t_2 = r_3 q_2 + t_3 \quad (28)$$

$$\dot{t}_2 = \dot{\bar{t}}_2 = r_3 \dot{\bar{q}}_2 + \dot{\bar{t}}_3 \quad (29)$$

$$t_1 = r_2 q_1 + t_2 \quad (30)$$

$$q_2 = q_{20} + \bar{q}_2 \quad (31)$$

Equations on q_1 from the 1st link:

$$q_1 = c_2 \dot{t}_2 + q_2 = c_2 (r_3 \dot{\bar{q}}_2 + \dot{\bar{t}}_3) + q_{20} + \bar{q}_2 = c_2 r_3 \dot{\bar{q}}_2 + c_2 \dot{\bar{t}}_3 + q_{20} + \bar{q}_2 \quad (32)$$

Equations on t_2 from the 1st link:

$$t_2 = r_3 q_2 + t_3 = r_3 q_{20} + r_3 \bar{q}_2 + t_{30} + \bar{t}_3 \quad (33)$$

The equation on t_1 :

$$\begin{aligned} t_1 &= r_2 q_1 + t_2 = r_2 (c_2 r_3 \dot{\bar{q}}_2 + c_2 \dot{\bar{t}}_3 + q_{20} + \bar{q}_2) + (r_3 q_{20} + r_3 \bar{q}_2 + t_{30} + \bar{t}_3) \\ &= c_2 r_2 r_3 \dot{\bar{q}}_2 + (r_2 + r_3) \dot{\bar{q}}_2 + (r_2 + r_3) q_{20} + c_2 r_2 \dot{\bar{t}}_3 + \bar{t}_3 + t_{30} \end{aligned} \quad (34)$$

The equation on $\dot{\bar{t}}_1$:

$$\dot{\bar{t}}_1 = c_2 r_2 r_3 \ddot{\bar{q}}_2 + (r_2 + r_3) \dot{\bar{q}}_2 + c_2 r_2 \ddot{\bar{t}}_2 + \dot{\bar{t}}_3 \quad (35)$$

The equation on q :

$$\begin{aligned} q &= c_1 \dot{t}_1 + c_2 \dot{t}_2 + q_2 \\ &= c_1 [c_2 r_2 r_3 \ddot{\bar{q}}_2 + (r_2 + r_3) \dot{\bar{q}}_2 + c_2 r_2 \ddot{\bar{t}}_2 + \dot{\bar{t}}_3] + c_2 (r_3 \dot{\bar{q}}_2 + \dot{\bar{t}}_3) + (q_{20} + \bar{q}_2) \\ &= c_1 c_2 r_2 r_3 \ddot{\bar{q}}_2 + (c_1 r_2 + c_1 r_3 + c_2 r_3) \dot{\bar{q}}_2 + \bar{q}_2 + q_{20} + c_1 c_2 r_2 \ddot{\bar{t}}_2 \\ &\quad + (c_1 + c_2) \dot{\bar{t}}_3 \end{aligned} \quad (36)$$

The equation on t :

$$\begin{aligned} t &= r_1 q + r_2 q_1 + r_3 q_2 + t_3 \\ &= b_1 \ddot{\bar{q}}_2 + b_2 \dot{\bar{q}}_2 + b_3 \bar{q}_2 + b_4 q_{20} + a_1 \ddot{\bar{t}}_2 + a_2 \dot{\bar{t}}_3 + a_3 \bar{t}_3 + a_4 t_{30} \end{aligned} \quad (37)$$

Equation for images:

$$(a_1 s^2 + a_2 s + a_3) Q_2(s) = -(b_1 s^2 + b_2 s + b_3) T_3(s) \quad (38)$$

Coefficients:

$$\begin{aligned} a_1 &= c_1 c_2 r_1 r_2 \\ a_2 &= c_1 r_1 + c_2 r_1 + c_2 r_2 \\ a_3 &= 1 \\ b_1 &= c_1 c_2 r_1 r_2 r_3 \\ b_2 &= c_1 r_1 r_2 + c_1 r_1 r_3 + c_2 r_1 r_3 + c_2 r_2 r_3 \end{aligned} \quad (39)$$

$$b_3 = r_1 + r_2 + r_3$$

Complex resistance $Z(s)$:

$$Z(s) = \frac{T_3(s)}{Q_2(s)} = \frac{a_1s^2 + a_2s + a_3}{-b_1s^2 - b_2s - b_3} \quad (40)$$

Frequency function of the circuit:

$$s \rightarrow j\Omega, j^2 = -1 \quad (41)$$

Frequency function of the circuit:

$$\begin{aligned} Z(s) &= \frac{T_3(s)}{Q_2(s)} = \frac{a_1s^2 + a_2s + a_3}{-b_1s^2 - b_2s - b_3} = \frac{-a_1\Omega^2 + a_2j\Omega + a_3}{b_1\Omega^2 - b_2j\Omega - b_3} \quad (42) \\ &= \frac{\left[-a_1b_1\Omega^4 + a_1b_3\Omega^2 - a_2b_2\Omega^2 + a_3b_1\Omega^2 - a_3b_3 + (a_2b_1\Omega^3 - a_1b_2\Omega^3) \right]}{(b_1\Omega^2 - b_3)^2 + b_2^2\Omega^2} \end{aligned}$$

We derive the real part of the complex resistance:

$$Re(j\Omega) = \frac{-a_1b_1\Omega^4 + a_1b_3\Omega^2 - a_2b_2\Omega^2 + a_3b_1\Omega^2 - a_3b_3}{(b_1\Omega^2 - b_3)^2 + b_2^2\Omega^2} \quad (43)$$

We derive the imaginary part of the complex resistance:

$$Im(j\Omega) = \frac{(a_2b_1\Omega^3 - a_1b_2\Omega^3 - a_2b_3\Omega + a_3b_2\Omega)}{(b_1\Omega^2 - b_3)^2 + b_2^2\Omega^2} j \quad (44)$$

We obtain the amplitude-frequency function of the energy circuit:

$$A(j\Omega) = \sqrt{Re(j\Omega)^2 + Im(j\Omega)^2} \quad (45)$$

Get the phase-frequency function of the energy circuit:

$$\varphi(j\Omega) = -arctg \frac{Im(j\Omega)}{Re(j\Omega)} \quad (46)$$

Construction of frequency characteristics of the circuit when changing at least three parameters. Parameter are calculated or found from the experiment. Are set by the input power of the circuit, $n_0 = 60 \text{ W}$, as well as the inlet pressure $P_0 = 300 \text{ kPa}$. Hire the pressure loss on the active resistance is assumed $5 \pm 10\%$.

$$V_0 = \frac{n_0}{P_0} = \frac{60}{300} = 0.2 \text{ l/s} \quad (47)$$

According to equation write the formula for r_1, r_2, r_3 :

$$\begin{aligned} r_1 &= \frac{P_0 * 0.1}{V_0^2} = \frac{0.1 \times 300}{0.2^2} = 750 \left[\frac{\text{kPa} \cdot \text{s}^2}{\text{lit}} \right] \quad (48) \\ r_2 &= 2r_1; \\ r_3 &= 4r_1; \end{aligned}$$

The mass of water depends on the volume of pipelines.

$$m = 15 \text{ kg} \quad (49)$$

The compliance is found for equation:

$$l = \frac{V_0 * 0.5}{P_0 * 0.3} = \frac{0.2 * 0.5}{300 * 0.3} = 0.0011 \left[\frac{\text{lit} \cdot \text{s}}{\text{kPa}} \right] \quad (50)$$

Algorithm for plotting graphs.

Table 1

CIRCUIT PARAMETERS

m, kg	$r_1, \frac{N}{m \cdot s}$	$r_2, \frac{N}{m \cdot s}$	$r_3, \frac{N}{m \cdot s}$	$l, \text{lit} \cdot \text{s}/\text{kPa}$	p_0, kPa	$V_{10}, \text{lit}/\text{s}$
15	750	1500	3000	0,0011	300	0.2
30	750	1500	3000	0,0011	300	0.2
15	375	750	1500	0,0011	300	0.2

Dependency graphs are plotted based on the input values. For the best perception of graphs values are taken only those that affect the dependence. The values obtained for the first stage of the energy circuit are shown in Table 2.

Table 2

RECEIVED INFORMATION FOR HYDRAULIC

Ω	$A_{j\Omega 1}$	$\varphi_{j\Omega 1}$	$A_{j\Omega 2}$	$\varphi_{j\Omega 2}$	$A_{j\Omega 3}$	$\varphi_{j\Omega 3}$
1	1.2544	0.6608	1.2542	0.6733	1.8148	1.0124
2	1.8753	1.0336	1.9290	1.0765	3.3068	1.3139
3	2.7313	1.2337	2.9147	1.2965	5.0083	1.4453
4	3.7723	1.3528	4.0366	1.4214	6.6127	1.5194
5	4.9237	1.4291	4.9854	1.4948	7.6950	1.5658
6	6.0502	1.4801	5.4975	1.5388	8.0085	-1.5457
7	6.9850	1.5149	5.5499	1.5656	7.6781	-1.5261
8	7.6017	1.5392	5.2983	-1.5595	7.0118	-1.5137
9	7.8672	1.5562	4.9109	-1.5494	6.2597	-1.5059
10	7.8345	1.5682	4.4949	-1.5434	5.5515	-1.5015

Based on the results of the calculation, the graphs of the amplitude frequency response and phase-frequency response and frequency response of the circuit are constructed. Further in these graphs are under construction:

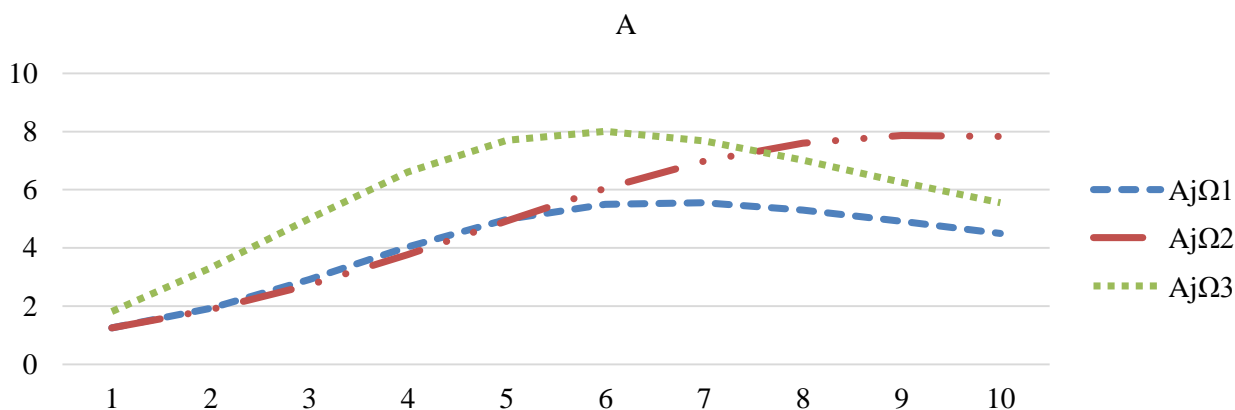


Figure 4. Amplitude frequency response

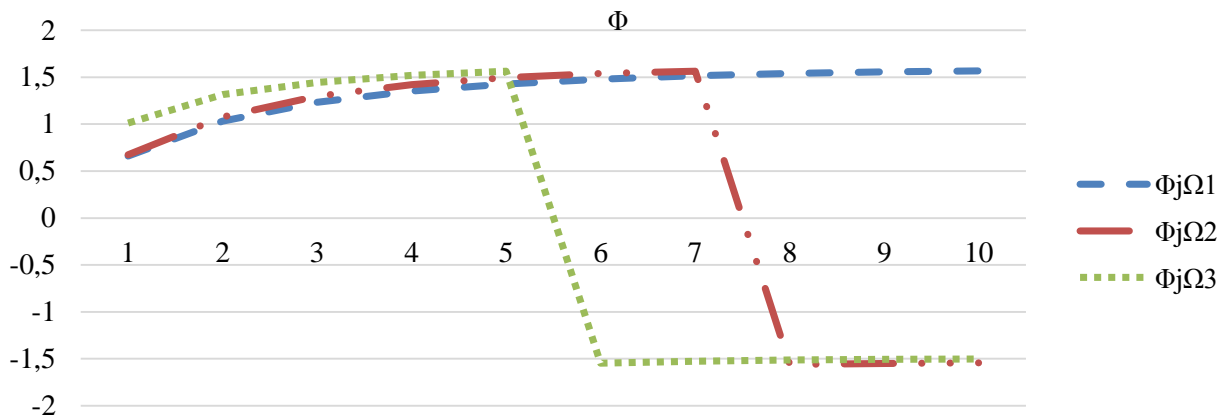


Figure 5. Phase frequency response

In the process of modeling the hydraulic power circuit, it is found that as the amplitude of the hydraulic circuit increases and the mass increases, the frequency decreases and then remains stable; as r decreases, the amplitude increases and the frequency decreases faster. The known conditions:

$$\begin{aligned} n_0 &= 1500W & (51) \\ t_0 &= 70^\circ\text{C} \\ \alpha_1 &: 800 - 1000 \\ \alpha_2 &: 10 - 15 \\ F &= 2m^2, \delta = 2mm \end{aligned}$$

By calculation:

$$q_0 = \frac{n_0}{t_0} = \frac{1500}{70} = 21.429 \left[\frac{W}{^\circ\text{C}} \right] \quad (52)$$

$$r_1 = \frac{1}{\alpha_1 F} = \frac{1}{1 \times 2} = 0.5 \left[\frac{kPa \cdot s^2}{lit} \right] \quad (53)$$

$$r_2 = \frac{\delta}{\lambda F} = \frac{0.002}{0.140 \times 2} = 7.143 \times 10^{-3} \left[\frac{kPa \cdot s^2}{lit} \right] \quad (54)$$

$$r_3 = \frac{1}{\alpha_2 F} = \frac{1}{0.010 \times 2} = 50 \left[\frac{kPa \cdot s^2}{lit} \right] \quad (55)$$

$$c_1 = \frac{\Delta q}{0.5t_0} = \frac{q - q_1}{0.5t_0} = \frac{2.1429}{0.5 \times 70} = 0.0612 \left[\frac{l}{s \cdot ^\circ\text{C}} \right] \quad (56)$$

$$c_2 = c_1 = 0.0612 \left[\frac{l}{s \cdot ^\circ\text{C}} \right] \quad (57)$$

The limit of change Ω is accept, $\Omega = 1 \dots 10$ rad/s.

Table 3

RECEIVED INFORMATION FOR HEAT TRANSFER

n_0, kw	$r_1, ^\circ\text{C}^2/w$	$r_2, ^\circ\text{C}^2/w$	$r_3, ^\circ\text{C}^2/w$	$c_1, w/^\circ\text{C}^2$	$c_2, w/^\circ\text{C}^2$	$t_0, ^\circ\text{C}$	$\lambda, \frac{kw}{m \cdot ^\circ\text{C}}$
1.5	0.5	7.143×10^{-3}	50	0,0612	0,0612	70	0.140
1.5	2	7.143×10^{-3}	50	0,0612	0,0612	70	0.140
1.5	4	7.143×10^{-3}	50	0,0612	0,0612	70	0.140

The dependency graph is drawn based on input values. For optimal graph perception, take only those values that affect dependencies. The obtained values for the first stage of heat transfer are shown in Table 4.

Table 4

VALUE AMPLITUDE FREQUENCY RESPONSE FOR ENERGY CIRCUIT

Ω	$A_{j\Omega 1}$	$\varphi_{j\Omega 1}$	$A_{j\Omega 2}$	$\varphi_{j\Omega 2}$	$A_{j\Omega 3}$	$\varphi_{j\Omega 3}$
1	0.0198	-0.0006	0.0195	-0.0092	0.0196	-0.0327
2	0.0199	-0.0012	0.0203	-0.0169	0.0222	-0.0502
3	0.0199	-0.0018	0.0215	-0.0225	0.0253	-0.0544
4	0.0201	-0.0024	0.0230	-0.0258	0.0282	-0.0522
5	0.0203	-0.0029	0.0246	-0.0274	0.0306	-0.0480
6	0.0204	-0.0035	0.0261	-0.0278	0.0325	-0.0435
7	0.0207	-0.0039	0.0276	-0.0274	0.0339	-0.0394
8	0.0209	-0.0044	0.0289	-0.0265	0.0349	-0.0358
9	0.0212	-0.0048	0.0302	-0.0254	0.0358	-0.0327
10	0.0214	-0.0052	0.0313	-0.0243	0.0365	-0.0299

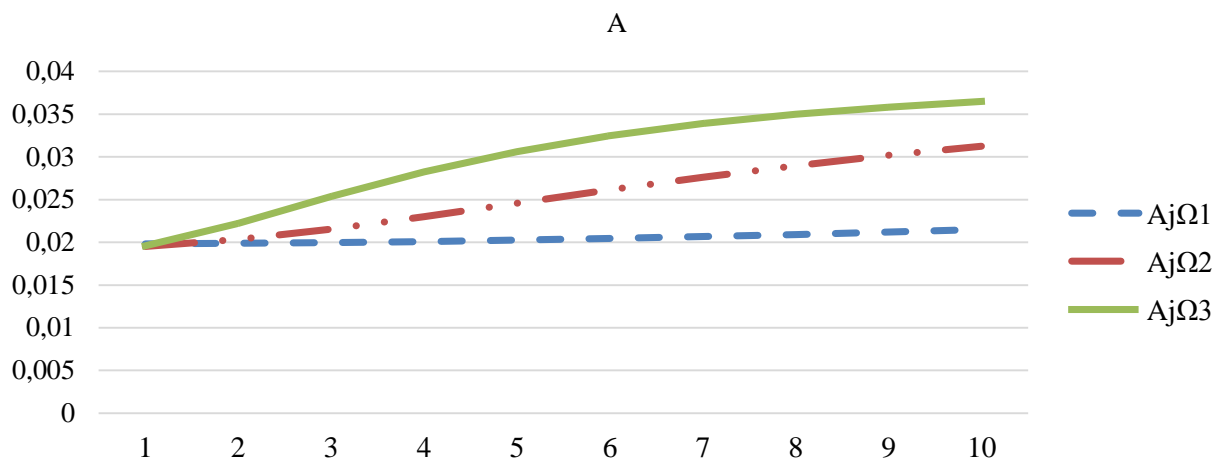


Figure 6. Amplitude frequency response

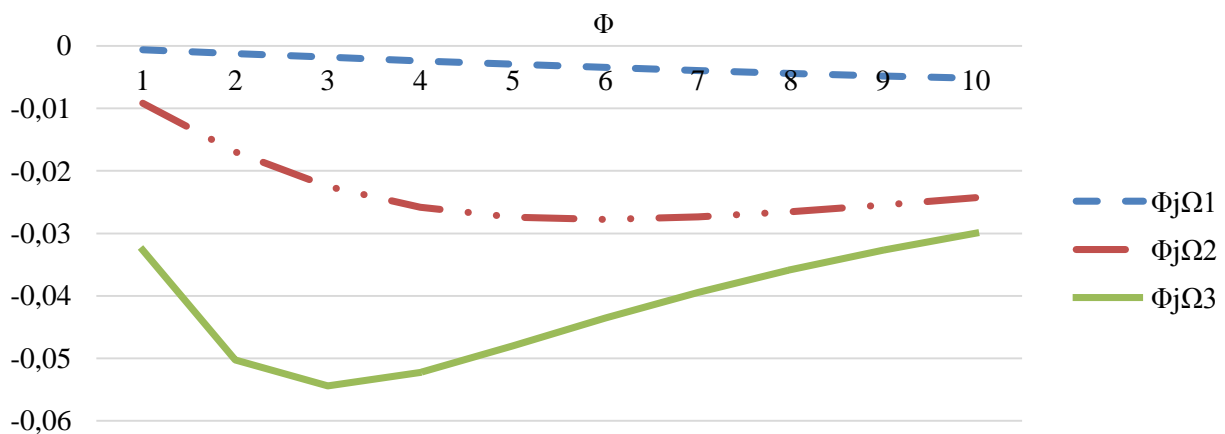


Figure 7. Phase frequency response

In the process of modeling the heat transfer process of the energy loop, it is found that the frequency response of the hydraulic loop decreases with increasing resistance and the amplitude increases.

Conclusion

In the course of the work, the problems associated with this work and possible solutions are described. A constructive scheme of the experimental device is proposed and the principle of its operation is described in detail. The power circuit of the device is drawn up, each link is explained. Complex impedance, frequency function, amplitude-frequency characteristic and phase-frequency characteristic are obtained by mathematical transformation of the power circuit. The frequency response of the circuit is constructed.

The description of the experimental setup is completed, energy circuits for hydraulics and heat transfer are compiled.

In the process of modeling the hydraulic power circuit, it is found that as the amplitude of the hydraulic circuit increases and the mass increases, the frequency decreases and then remains stable; as r decreases, the amplitude increases and the frequency decreases faster.

In the process of modeling the heat transfer process of the energy loop, it is found that the frequency response of the hydraulic loop decreases with increasing resistance and the amplitude increases.

According to the resulting graphs, one can trace the relationship between two different properties. It can be seen from the graph that for a particular r value, we reach the frequency maximum faster.

References:

1. Li, Y., Ru, X., Yang, M., Zheng, Y., Yin, S., Hong, C., ... & Shao, Z. (2024). Flexible silicon solar cells with high power-to-weight ratios. *Nature*, 626(7997), 105-110. <https://doi.org/10.1038/s41586-023-06948-y>
2. Xu, R., Long, Y., & Wang, D. (2018). Effects of rotating speed on the unsteady pressure pulsation of reactor coolant pumps with steam-generator simulator. *Nuclear Engineering and Design*, 333, 25-44. <https://doi.org/10.1016/j.nucengdes.2018.03.021>
3. Barrio, R., Parrondo, J., & Blanco, E. (2010). Numerical analysis of the unsteady flow in the near-tongue region in a volute-type centrifugal pump for different operating points. *Computers & Fluids*, 39(5), 859-870. <https://doi.org/10.1016/j.compfluid.2010.01.001>
4. Li, D., Gong, R., Wang, H., Xiang, G., Wei, X., & Liu, Z. (2015). Dynamic analysis on pressure fluctuation in vaneless region of a pump turbine. *Science China Technological Sciences*, 58, 813-824. <https://doi.org/10.1007/s11431-014-5761-4>
5. Pei, J., Yuan, S., Benra, F. K., & Dohmen, H. J. (2012). Numerical prediction of unsteady pressure field within the whole flow passage of a radial single-blade pump. <https://doi.org/10.1115/1.4007382>
6. Pei, J., Yuan, S., & Yuan, J. (2013). Numerical analysis of periodic flow unsteadiness in a single-blade centrifugal pump. *Science China Technological Sciences*, 56, 212-221. <https://doi.org/10.1007/s11431-012-5044-x>
7. Barrio, R., Blanco, E., Parrondo, J., González, J., & Fernández, J. (2008). The effect of impeller cutback on the fluid-dynamic pulsations and load at the blade-passing frequency in a centrifugal pump. <https://doi.org/10.1115/1.2969273>
8. Sun, J., & Tsukamoto, H. (2001). Off-design performance prediction for diffuser pumps. *Proceedings of the Institution of Mechanical Engineers, Part A: Journal of Power and Energy*, 215(2), 191-201. <https://doi.org/10.1243/0957650011538460>

9. Wang, H., & Tsukamoto, H. (2003). Experimental and numerical study of unsteady flow in a diffuser pump at off-design conditions. *J. Fluids Eng.*, 125(5), 767-778. <https://doi.org/10.1115/1.1603305>
10. Parrondo-Gayo, J. L., Gonza'lez-Pe' rez, J., & Ferna' ndez-Francos, J. N. (2002). The effect of the operating point on the pressure fluctuations at the blade passage frequency in the volute of a centrifugal pump. *J. Fluids Eng.*, 124(3), 784-790. <https://doi.org/10.1115/1.1493814>
11. Benra, F. K. (2006). Numerical and experimental investigation on the flow induced oscillations of a single-blade pump impeller. <https://doi.org/10.1115/1.2201629>
12. Long, Y., Zhang, M., Qiang, Z., & Zhu, R. (2023). Effect of non-uniform inflow on the internal flow and hydrodynamic characteristics of a small modular reactor coolant pump. *Annals of Nuclear Energy*, 192, 109984. <https://doi.org/10.1016/j.anucene.2023.109984>
13. Zhang, M., Zhang, W., Zhang, R., Guo, X. A., Zhu, R., Yuan, S., & Long, Y. (2024, February). Study on unsteady characteristics of the reactor coolant pump under non-uniform inflow. In *Journal of Physics: Conference Series* (Vol. 2707, No. 1, p. 012052). IOP Publishing. <https://doi.org/10.1088/1742-6596/2707/1/012052>

Список литературы:

1. Li Y., Ru X., Yang M., Zheng Y., Yin S., Hong C., Shao Z. Flexible silicon solar cells with high power-to-weight ratios // *Nature*. 2024. V. 626. №7997. P. 105-110. <https://doi.org/10.1038/s41586-023-06948-y>
2. Xu R., Long Y., Wang D. Effects of rotating speed on the unsteady pressure pulsation of reactor coolant pumps with steam-generator simulator // *Nuclear Engineering and Design*. 2018. V. 333. P. 25-44. <https://doi.org/10.1016/j.nucengdes.2018.03.021>
3. Barrio R., Parrondo J., Blanco E. Numerical analysis of the unsteady flow in the near-tongue region in a volute-type centrifugal pump for different operating points // *Computers & Fluids*. 2010. V. 39. №5. P. 859-870. <https://doi.org/10.1016/j.compfluid.2010.01.001>
4. Li D., Gong R., Wang H., Xiang G., We X., Liu Z. Dynamic analysis on pressure fluctuation in vaneless region of a pump turbine // *Science China Technological Sciences*. 2015. V. 58. P. 813-824. <https://doi.org/10.1007/s11431-014-5761-4>
5. Pei J., Yuan S., Benra F. K., Dohmen H. J. Numerical prediction of unsteady pressure field within the whole flow passage of a radial single-blade pump. 2012. <https://doi.org/10.1115/1.4007382>
6. Pei J., Yuan S. Q., Yuan J. P. Numerical analysis of periodic flow unsteadiness in a single-blade centrifugal pump // *Science China Technological Sciences*. 2013. V. 56. P. 212-221. <https://doi.org/10.1007/s11431-012-5044-x>
7. Barrio R., Blanco E., Parrondo J., González J., Fernández, J. The effect of impeller cutback on the fluid-dynamic pulsations and load at the blade-passing frequency in a centrifugal pump. 2008. <https://doi.org/10.1115/1.2969273>
8. Sun J., Tsukamoto H. Off-design performance prediction for diffuser pumps // *Proceedings of the Institution of Mechanical Engineers, Part A: Journal of Power and Energy*. 2001. V. 215. №2. P. 191-201. <https://doi.org/10.1243/0957650011538460>
9. Wang H., Tsukamoto H. Experimental and numerical study of unsteady flow in a diffuser pump at off-design conditions // *J. Fluids Eng.* 2003. V. 125. №5. P. 767-778. <https://doi.org/10.1115/1.1603305>
10. Parrondo-Gayo J. L., Gonza'lez-Pe' rez J., Ferna' ndez-Francos J. The effect of the operating point on the pressure fluctuations at the blade passage frequency in the volute of a centrifugal pump // *J. Fluids Eng.* 2002. V. 124. №3. P. 784-790. <https://doi.org/10.1115/1.1493814>

11. Benra, F. K. (2006). Numerical and experimental investigation on the flow induced oscillations of a single-blade pump impeller. <https://doi.org/10.1115/1.2201629>
12. Long, Y., Zhang, M., Qiang, Z., & Zhu, R. (2023). Effect of non-uniform inflow on the internal flow and hydrodynamic characteristics of a small modular reactor coolant pump. *Annals of Nuclear Energy*, 192, 109984. <https://doi.org/10.1016/j.anucene.2023.109984>
13. Zhang, M., Zhang, W., Zhang, R., Guo, X. A., Zhu, R., Yuan, S., & Long, Y. (2024, February). Study on unsteady characteristics of the reactor coolant pump under non-uniform inflow. In *Journal of Physics: Conference Series* (Vol. 2707, No. 1, p. 012052). IOP Publishing. <https://doi.org/10.1088/1742-6596/2707/1/012052>

Работа поступила
в редакцию 28.04.2024 г.

Принята к публикации
06.05.2024 г.

Ссылка для цитирования:

Han Wang, Maltsev S. Energy Circuit of a Thermal Circuit with a Direct-acting Regulator with a Capacity of 1 MW in Pulsating Mode // Бюллетень науки и практики. 2024. Т. 10. №6. С. 372-383. <https://doi.org/10.33619/2414-2948/103/40>

Cite as (APA):

Han, Wang, & Maltsev, S. (2024). Energy Circuit of a Thermal Circuit with a Direct-acting Regulator with a Capacity of 1 MW in Pulsating Mode. *Bulletin of Science and Practice*, 10(6), 372-383. <https://doi.org/10.33619/2414-2948/103/40>